Journal of Fluorine Chemistry 162 (2014) 78–89

Contents lists available at ScienceDirect

Journal of Fluorine Chemistry

journal homepage: www.elsevier.com/locate/fluor

Synthesis, characterization and effect of the fluorine substitution on the redox reactivity and *in vitro* anticancer behaviors of *N*-polyfluorophenyl-3,5-di-*tert*-butylsalicylaldimines and their Cu(II) complexes

V.T. Kasumov [a,*], F. Süzergöz [b], E. Sahin [c], Ö. Çelik [d], M. Aslanoğlu [a]

[a] Chemistry Department, Faculty of Science & Art, Harran University, 630190 Sanliurfa, Turkey
[b] Biology Department, Faculty of Science & Art, Harran University, 630190 Sanliurfa, Turkey
[c] Department of Chemistry, Ataturk University, Faculty of Science, TR-25240 Erzurum, Turkey
[d] Physics Department, Faculty of Education, Dicle University, 212800 Diyarbakr, Turkey

ARTICLE INFO

Article history:
Received 10 November 2013
Received in revised form 25 March 2014
Accepted 26 March 2014
Available online 3 April 2014

Keywords:
Polyfluorinated
Cu(II)–phenoxyl radicals
Spectroscopy
Anticancer

ABSTRACT

A series of new polyfluorinated bis(*N*-$C_6F_nH_{5-n}$3,5-^{t}Bu$_2$salicylaldiminato)Cu(II) [n = 2; 2,4-$F_2C_6H_3$-3,5-DTBS (**1**), 2,5-$F_2C_6H_3$-3,5-DTBS (**2**), 2,6-$F_2C_6H_3$-3,5-DTBS (**3**); n = 3; 2,3,4-$F_3C_6H_2$-3,5-DTBS (**4**), n = 4; 2,3,5,6-F_4C_6H-3,5-DTBS (**5**), n = 5; 2,3,4,5,6-F_5C_6-3,5-DTBS (**6**); where 3,5-DTBS is 3,5-^{t}Bu$_2$salicylaldiminato] with *N*-polyfluorophenyl-3,5-di-*tert*-butylsalicylaldi-mines (**HL^1**–**HL^6**) have been synthesized. Their structure, chemical and electrochemical redox-reactivity as well as cytotoxic activity of these compounds were characterized by analytical, spectroscopic (UV/vis, FT-IR, ^{19}F NMR and EPR), magnetic, CV techniques and MTT assay. The *in situ* UV/Vis study have shown that the redox behavior of **1**–**6** and their Cu–phenoxyl radicals (**1**$^{\bullet+}$–**6**$^{\bullet+}$ and **1**$^{\bullet\bullet+}$–**6**$^{\bullet\bullet+}$) depend on the number and positions of F atoms on the aniline ring as well as of the nature of solvent. The *in vitro* cytotoxic activity studies of **HL^1**–**HL^6** and **1**–**6** against K562 cell lines indicate that the **HL^1**, **HL^4**–**HL^6** and their corresponding complexes (**1**, **4**–**6**) exhibited higher cytotoxic activity than **HL^2**, **HL^3** and their complexes. Compounds **1**, **4** and **5** are more cytotoxic than their respective ligands.

1. Introduction

The design, synthesis and structural characterization of salicylaldimine complexes bearing bulky *tert*-butyl groups are a subject of current interest due to their interesting structural, spectral, magnetic, catalytic, and redox properties, use as models for enzymes and various theoretical interests [1–4]. Phenoxyl radicals have been identified as an essential component of several metalloenzyme active sites [3]. The discovery of Cu(II)–phenoxyl radical centers in the active site of Cu(II)-containing enzymes (galactose and glyoxal oxidases and other metal enzymes) [3,4] has stimulated the development of various transition metal chelates with redox-active noninnocent ligands which exhibits the ability to form the directly coordinated M(II)/(III)–phenoxyl radical complexes [1–7].

While one of the unique properties of first row transition metal complexes with non-innocent redox-active phenoxyimine ligands bearing bulky *tert*-butylated phenol fragments is their ability to form stable metal(II)/(III)–phenoxyl type ligand-radical complexes [3–6], the early 4- and 5-group transition metal complexes with redox-active polyfluorinated phenoxyimine ligands have been widely used as controlled living olefin polymerization catalysts [8–18]. Depending on the number and position, a fluorine substitution not only affects the electronic and structural properties of the molecule itself but also gives rise to uncommon intermolecular behavior [19,20]. It is well known that because of fluorine's atom strong electron-withdrawing effect and its small size, the presence of fluorine in a molecule exerts a large influence on physicochemical properties such as lipophilicity, acidity or basicity, changes quite drastically the charge distribution in compounds, thereby altering their biological effects [19–21]. Literature survey revealed that while the catalytic activities of the polyfluorinated sterically hindered phenoxyimine ligands of early 4- and 5-group transition metal complexes are widely studied, the redox reactivity and biological features of the transition metal complexes are scarcely

* Corresponding author. Tel.: +90 414 318 3588/+90 414 3440020 1265; fax: +90 414 3180046/+90 4143440051.
E-mail address: vkasumov@harran.edu.tr (V.T. Kasumov).

http://dx.doi.org/10.1016/j.jfluchem.2014.03.011
0022-1139/

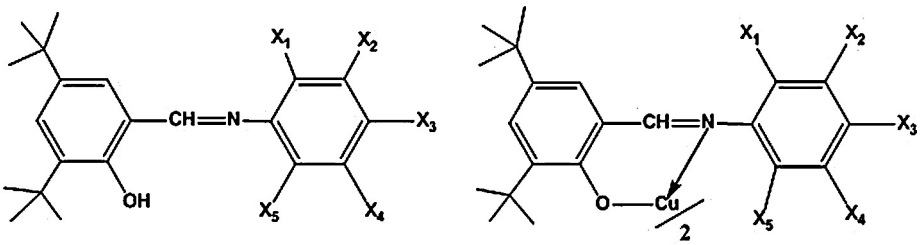

HL^1 : $X_1 = X_3 = F, X_2 = X_4 = X_5 = H$ — $Cu(L^1)_2$ (1)
HL^2 : $X_1 = X_4 = F, X_2 = X_3 = X_5 = H$ — $Cu(L^2)_2$ (2)
HL^3 : $X_1 = X_5 = F, X_2 = X_3 = X_4 = H$ — $Cu(L^3)_2$ (3)
HL^4 : $X_1 = X_2 = X_3 = F, X_4 = X_5 = H$ — $Cu(L^4)_2$ (4)
HL^5 : $X_1 = X_2 = X_4 = X_5 = F, X_3 = H$ — $Cu(L^5)_2$ (5)
HL^6 : $X_1 = X_2 = X_3 = X_4 = X_5 = F$ — $Cu(L^6)_2$ (6)

Scheme 1. Chemical structure of the ligands (HL^1–HL^6) and their bis-ligands copper(II) complexes (**1**–**6**).

investigated. The fact that introduction of fluorine atom on molecule exerts significant changes in its physicochemical and biological properties, in the course of our interest on the structure and redox reactivity of the transition metal complexes with di-*tert*-butylphenol functionalized salicylaldimines [22,23], we have decided to study the effects of fluorine atoms on the redox reactivity and anticancer behavior of the polyfluorinated redox-active 3,5-di-*tert*butylsalicylaldimine ligands and their transition metal(II) complexes. Since the presented ligands contain sterically hindered phenol and polyfluorinated aniline fragments, one can suggest that these ligands would possess both antioxidant and antitumor efficiency [24]. It is well known that sterically hindered phenolic compounds along with antioxidant activity also exhibit anti-inflammatory, antimicrobial, hypolipidemic, antimutagenic and anticarcinogenic effects [25a–c]. The incorporation of F atoms on organic compounds also enhances their biological activity, chemical reactivity, physicochemical properties as well as their various material properties. In addition, F or CF_3 substituent also improves lipophilicity, and suppresses metabolic detoxification processes to increase the *in vivo* lifetime of drugs [25d].

In this context, we wish to report the synthesis, spectroscopic characterization, crystal structure, chemical redox-reactivity and antitumor behavior of some *N*-polyfluorophenyl-3,5-di-*tert*-butyl-salicylidene ligands (HL^1–HL^6) Cu(II) complexes (**1**–**6**) (Scheme 1). The crystal structure and preliminary redox behavior of **4** and HL^1–HL^6 ligands and their palladium(II) complexes have recently been reported by us [23]. The synthesis, IR and ^{13}C NMR characteristics of HL^1–HL^6 and other numerous fluorinated salicylaldimines early have been reported [8–17].

2. Results and discussion

2.1. Structure study

Despite of our efforts to crystallize the fluorinated **1**–**3** and **6** complexes, no crystals suitable for X-ray measurements were obtained. The molecular structure of **5** including atom-numbering is shown in Fig. 1. Crystal data and additional data collection parameters and refinement details are presented in Table 1. Selected bond lengths and angles of **5** are listed in Table 2.

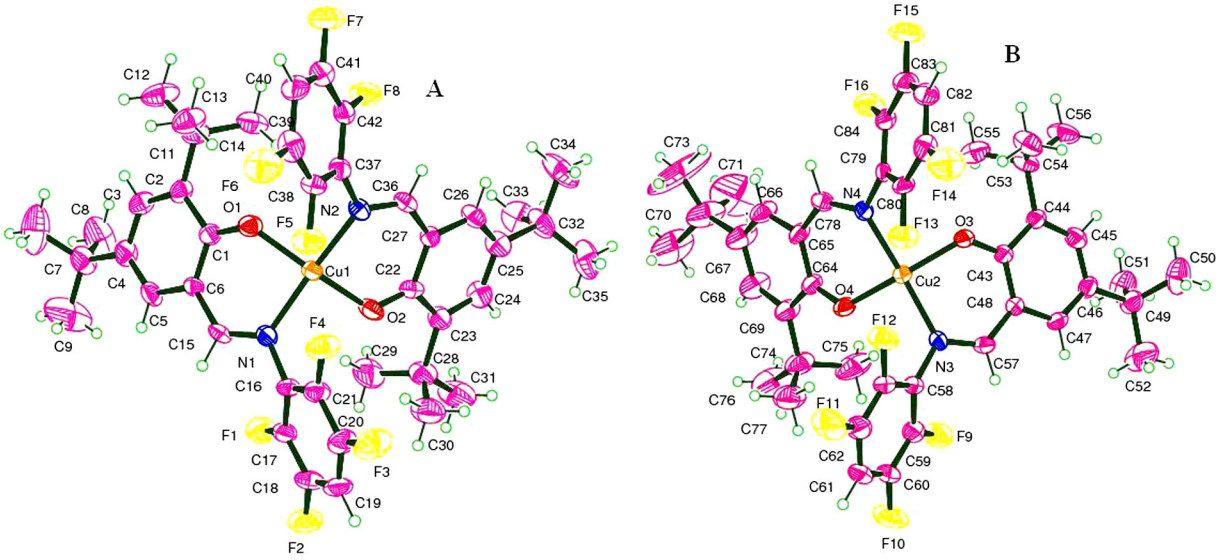

Fig. 1. Molecular structures of the two independent complexes ((A) and (B)) in the crystal structure of **5** showing the atom numbering scheme. Thermal ellipsoids of non-hydrogen atoms are drawn at the 50% probability level. H atoms are presented by arbitrarily small spheres.

Table 1
Crystal data and structure refinement for compound **5**.

Formula	$C_{84}H_{88}$ $N_4O_4F_{16}Cu_2$
Formula weight	1649.09
Crystal system	Monoclinic
Space group (no.)	*P*121/c1
a = 23.7519(7) Å	
b = 34.2504(9) Å	*β* = 93.392(1)°
c = 10.7424(3) Å	
Cell volume (Å^3)	8723.8(4)
Calculated density (Mg/m^3) 1.255	
Cell formula units *Z*	19
μ (Mo *K*α) (mm^{-1})	3.931
T (K)	293(2)
Crystal description	Prism
Color	Red
Crystal sizes (mm)	0.30 × 0.20 × 0.15
Radiation Mo *K*α (λ = Å)	0.71073
θ_{min}–θ_{max} (°)	2.0–21.6
F(000)	3416
Index rangers	$-24 \le h \le 24$, $-35 \le k \le 35$, $-11 \le l \le 10$
Reflection collected	74,602
Num. of refined parameters 1008	
Num. of reflection used	9664
Observed data ($I > 2\sigma(I)$)	6972
R [F2 > 2σ(F2)]	0.072
Rw (F2)	0.100
$w = 1/[\sigma_2(Fo_2) + (0.0000P)^2 + 20.8677P]$, where $P = (Fo^2 + 2Fc^2)s/3$	
Goodness-of-fit on F2	1.106
$(\rho\Delta)_{max}$ (eÅ^{-3})	0.307
$(\rho\Delta)_{min}$ (eÅ^{-3})	−0.318

Hydrogen bonds and short intramolecular contacts are given in Table 3. X-ray diffraction analysis of **5** revealed that there are two crystallographically independent molecules (**A** and **B**) in the asymmetric unit (Fig. 1). These molecules are mirror images of each other with virtually identical bond lengths and angles (Table 2). Each Cu(II) center is coordinated by two imine nitrogens and two phenolate oxygens from two **HL^5** molecules, adopting a slightly distorted square planar *trans*-[CuN_2O_2] geometry. The average Cu–O and Cu–N lengths of 1.884(5) and 1.980(4) Å in **A** and **B**, respectively, correspond well with those reported for nonfluorinated bis-salicylaldimine copper(II) complexes [22e,23b,26–29]. The two diagonal O2–Cu1–O1 and N2–Cu1–N1 angles of 160.94(2)° and 166,76 (2)°, respectively, are less than 180° as a result of tetrahedral distortion around Cu(II) center. Similar values were also found for complex **B** (Table 2). Selected data for hydrogen-bonding interactions are given in Table 3. Although the C–O, CH=N, Cu–O and Cu–N bond lengths of **A** and **B** complex molecules are very close to each other, the dihedral angles

Table 2
Selected bond lengths (Å), bond angles (°) and torsion angles (°) for compound **5**.

Bond lengths		Bond angles		Torsion angle (°)	
Cu1–O1	1.892(4)	O2–Cu1–O1	160.94(17)	O2–Cu1–N2 –C37	161.2(4)
Cu1–O2	1.877(4)	O2–Cu1–N1	90.05(17)	O1–Cu1–N1–C16	−158.1(4)
Cu1–N1	1.980(4)	O1–Cu1–N1	91.02(17)	N2–Cu1–O1–C1	150.2(4)
Cu1–N2	1.980(4)	O2–Cu1–N2	91.77(17)	O2–Cu1–O1–C1	50.3(7)
Cu2–O3	1.888(3)	O1–Cu1–N2	91.52(17)	N1–Cu1–O1–C1	−42.8(4)
Cu2–O4	1.884(4)	N1–Cu1–N2	166.76(18)	O1–Cu1–O2–C22	63.1(7)
Cu2–N3	1.982(4)	O4–Cu2–O3	158.36(17)	N1–Cu1–O2–C22	156.4(4)
Cu2–N4	1.981(4)	O4–Cu2–N4	92.03(16)	N2–Cu1–O2–C22	−36.7(4)
C1–O1	1.317(4)	O3–Cu2–N4	90.85(16)	O4–Cu2–N4–C79	161.9(4)
C22–O2	1.305(4)	O4–Cu2–N3	91.08(16)	O4–Cu2–O3–C43	−56.8(6)
C15–N1	1.299(4)	O3–Cu2–N3	91.62(16)	N4–Cu2–O4–C64	38.9(4)
C36–N2	1.299(4)	N4–Cu2–N3	165.09(18)	O3–Cu2–O4–C64	−58.5(6)
C43–O3	1.313(3)			N3–Cu2–O4–C64	−155.6(4)
C64–O4	1.315(3)			O3–Cu2–N3–C58	158.8(4)
C57–N3	1.299(4)			N4–Cu2–O3–C43	−154.5(4)
C78–N4	1.299(4)			N3–Cu2–O3–C43	40.3(4)

Table 3
Geometrical parameters (Å) for hydrogen bonds and short intramolecular contacts.

D–H···A	D–H (Å)	D–A (Å)	H···A (Å)	D–H···A (°)
C1–H15···F1^{i}	0.936(5)	2.866(7)	2.397(4)	110.80(4)
C77–H77B···F2	0.960(8)	3.426(8)	2.912(4)	114.73(5)
C36–H36···F8^{i}	0.897(5)	2.862(7)	2.343(5)	116.83(4)
C57–H57···F9^{i}	0.930(6)	3.328(7)	2.815(3)	115.91(4)
C19–H19···F12^{i}	0.960(4)	2.862(7)	2.296(4)	117.00(3.0)
C78–H78···F16^{i}	0.960(6)	2.830(7)	2.220(5)	117.67(3.0)
C13–H13B···O1^{i}	0.960(6)	3.029(7)	2.395(3)	123.22(4)
C14–H14B···O1^{i}	0.960(7)	3.010(7)	2.378(3)	123.01(4)
C29–H29C···O2^{i}	0.960(7)	3.021(8)	2.372(4)	124.49(4)
C55–H55B···O3^{i}	0.960(7)	2.976(7)	2.326(4)	124.41(4)
C75–H75C···O4^{i}	0.960(8)	3.005(8)	2.367(3)	123.46(4)
C77–H77C···O4^{i}	0.960(7)	2.991(8)	2.345(4)	124.11(4)
C5–H5···F7^{ii}	0.930(6)	3.303(7)	2.805(4)	114.72(4)
C15–H15···F7^{ii}	0.936(5)	3.320(7)	2.668(4)	127.27(3.0)
C30–H30A···F10^{iv}	0.960(8)	3.421(8)	2.822(4)	121.29(4)
C13–H13B···F7^{v}	0.960(6)	3.260(7)	2.910(4)	102.79(4)
C54–H54B···F15^{v}	0.960(6)	3.272(7)	2.779(4)	112.72(4)
C13–H13B···Cg(4)i	0.960(6)	3.673(7)	2.9379	134.26
C30–H30C···Cg(2)^{i}	0.960(8)	3.584(7)	2.8120	138.02
C54–H54C···Cg(8)^{i}	0.960(6)	3.704(7)	2.9458	136.83
C77–H77C···Cg(6)^{i}	0.960(7)	3.828(7)	3.0318	141.15
C33–H33C···Cg(1)^{vi}	0.960(7)	3.950(7)	3.0696	153.16

Symmetry codes: (i) *x*, *y*, *z*, (ii) *x*, +*y*, +*z* + 1, (iii) *x*, −*y* + 1/2, +*z* − 1/2, (iv) *x*, +*y*, +*z* − 1, (v) *x*, −*y* + 1/2, +*z* + 1/2, (vi) −*x*, −*y*, −*z*.

between C16–C21/C37–C43 phenyl planes in **A** and between C58–C63/C79–C84 phenyl planes in **B** are 30.30(1)° and 57.56(2)°, respectively. On the other hand, the dihedral angles between the two salicylidene planes in **A** (C1–C6/C22–C27) and in **B** (C43–C48/C64–C69) are 75.4 (2)° and 76.8(2)°, respectively. The dihedral angles between phenyl/salicylidene planes, C37–C42/C22–C27 [61.10(1)°] and C1–C6/C16–C21 [26.88(1)°] in **A**, are quite different. However, the same dihedral angles in **B** [(C64–C69/C79–C84 = 29.1/(3)° and C58–C63/C43–C48 = 31.4(3)°] are close to each other. The two **A** and **B** complexes are linked by two strong intermolecular C–H···F hydrogen bonds [(C19–H···F12–C12 (2.296(4) Å) and C77–H77···F2C18 (2.912(4) Å] to form a dimer in which the Cu···Cu distance is 9.350 Å (Fig. 2). Cu–O and Cu–N bond lengths are virtually the same as those in **A** and **B** (Table 2). O–Cu–N bond angles of **A** differ slightly from 90°. The dihedral angles between the two planes O1–Cu1–N1 and O2–Cu1–N2 in **A** and between O3–Cu2–N3 and O4–Cu2–N4 in **B** are 22.98° and 25.98°, respectively. These data compares with 0° for a perfect square-planar arrangement and 90° for a perfect tetrahedral arrangement.

In the crystal structure, there are many intramolecular and intermolecular C–H···F and C–H···O type H-bonding interactions (Table 3). In the crystal packing of **5**, there are also a weak intermolecular and intramolecular C–H···Cg (π-ring) type stacking interactions. These intermolecular interactions are responsible for constructing of the crystal structure of the complex **5**.

2.2. Spectroscopic properties of *1–6*

The analytical, IR, UV/vis and ^{1}H NMR spectroscopic characteristics and chemical oxidation behaviors of the **HL^x** were previously reported [8–12, 23c]. The ^{19}F NMR spectroscopic data of **HL^x** and selected IR data of the complexes **1–6** along with their interpretation are presented in Section 4. It is worthwhile noting that the electronic spectra of the polyfluorinated **HL^x** ligands unlike their non-fluorinated dimethyl [30a] and dimethoxy [30b] substituted analogs, as well as monosubstituted *ortho*- and *para*-(F, Cl, Br, OCH_3, CH_3 and $(CH_3)_3C$) analogs [30c] do not exhibit any absorption band even in the concentrated methanolic and ethanolic solvents in the λ > 365 nm region [22].

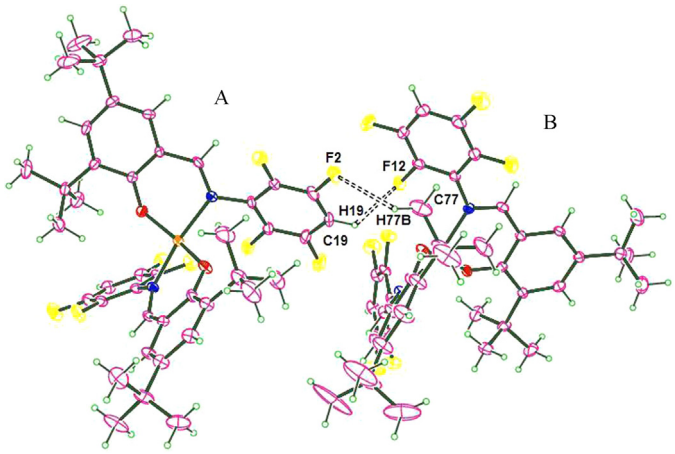

Fig. 2. The structure of **5**, with displacement ellipsoids drawn at the 50% probability level for the H-bonded dimers. Dotted lines indicate hydrogen bonds. Molecules A and B are mirror images.

The IR spectra of all compounds **1–6** exhibit sharp bands in the region of 2860–2950 cm^{-1} due to the asymmetric and symmetric ν(C–H) stretching vibrations of the $C(CH_3)_3$ groups. The strong bands observed in the range 1602–1616 cm^{-1} were assigned to νC=N stretching vibrations of the **1–6** complexes [31a]. These bands were shifted to lower frequencies relative to those of free **HL^1–HL^6** ligands (1622–1630 cm^{-1}), indicating that the ligands are coordinated through the imines nitrogen atoms to copper(II). A weak broad feature centered at 2700–2800 cm^{-1}, due to ν(OH) of the intramolecularly H-bonded OH···N in **HL^1**–HL^6, disappears in the spectra of all the complexes. These observations suggest the coordination of the ligands *via* imine nitrogen atom and deprotonated phenolic oxygen atom to Cu(II). The appearance of new strong band at 1526–1533 cm^{-1}, attributable to the coupling of ν(C–O) + ν(C=C–O) stretching mode [31b], and moderate intensity new bands at 475–560 cm^{-1} assignable to the ν(Cu–O) and ν(Cu–N) [31a], further confirmed the coordination of ligands through phenolic oxygen and imine nitrogen atoms to the Cu(II) metal ion.

The electronic spectra of **1–6** complexes in $CHCl_3$, MeCN and DMF solutions exhibit very similar two intense doublets in the region 206–365 nm, assignable to intraligand $\pi \rightarrow \pi^*$ and $n \rightarrow \pi^*$ [32,33], intense absorption band at 412–425 nm (ε = 3.06–4.02 $(M\ cm)^{-1}$) (Table 4) and unresolved broad shoulder at 650–670 nm. The band at 412–425 nm according to its highest molar extinction coefficients has been assigned to the phenolate-to-Cu(II) $[O(p_\pi) \rightarrow \left(d_{x^2-y^2}\right)Cu(II)]$ [3–5] charge transfer (LMCT). The unresolved broad shoulders at 650–670 nm are attributed to convolution of three allowed d–d transitions $\left[{}^2B_{1g} \rightarrow {}^2A_{1g}\left(d_{x^2-y^2} \rightarrow d_z^2\right),\ {}^2B_{1g} \rightarrow {}^2B_{2g}\left(d_{x^2-y^2} \rightarrow d_{xy}\right)\ and\ {}^2B_{1g} \rightarrow {}^2E_g\left(d_{x^2-y^2} \rightarrow d_z^2\right)\right]$, in a tetrahedrally distorted square-planar geometries [33].

The room temperature (r.t.) effective magnetic moment (μ_{eff}) of **1** (1.65μ_B) is lower than that expected for magnetically non interacting spin only value of 1.73μ_B, suggesting the existence of a weak intermolecular antiferromagnetic interaction between neighboring molecules of **1** [34]. The μ_{eff} values found for **2** (1.72μ_B) and **4–6** (1.80–1.86μ_B) (Section 4.4) are typical for magnetically non interacting Cu(II) centers in square planar or slightly distorted square-planar mononuclear geometries [34,35a]. The r.t. magnetic moment of **3** (2.08μ_B) is typical for significantly tetrahedrally distorted Cu(II) complexes [34].

Solid state and solution spectral spin Hamiltonian parameters of **1–6** complexes are listed in Table 5. The solid-state EPR spectra of **1–6** at 300 and 173 K are characterized by an axial g tensors with $g_{II} > g_\perp > g_e$, indicating that the copper site has a $d_{x^2-y^2}$ or d_{xy} ground state characteristic for tetrahedral, square-planar or a slightly distorted square planar geometries of the Cu(II) ion [35]. No half-field $\Delta Ms = \pm 2$ signals typical for binuclear triplet-state species were observed, ruling out the possibility of the dimeric forms. The EPR spectra of **1**, **3** and **4** exhibit one broadened anisotropic signal (Fig. 3) with g_{av} = 2.110, g_{av} = 2.116 and g_{av} = 2.079, respectively, which is attributable to dipolar interaction between crystallographically nonequivalent Cu(II) centers in the solid state [35a]. On the other hand, the powder spectra of **2**, **5** and **6** (Fig. 3c) complexes showed three well resolved copper(II) hyperfine components in the g_{II} region (Table 5) at r.t., indicating that the Cu(II) centers are magnetically diluted in these complexes [23,35].

The r.t. EPR spectra of **1–6** in $CHCl_3$ solution exhibit a typical four-line pattern without ^{14}N-shfs resolutions on the high-field components. The cryogenic solution spectra recorded in $CHCl_3$ glasses at 173 of all **1–4** and that of **5** and **6** complexes at 120 K, exhibit usual $g_{II} > g_\perp > 2.04$ and $A_{II} \gg A$ pattern consistent with a $d_{x^2-y^2}$ ground state in a tetrahedrally distorted or square-planar copper(II) centers (Table 5) [35]. The representative frozen glass

Table 4
UV/vis spectral data for **1–6** complexes and their oxidized intermediates.

Complex	Solvent	Electronic spectra, λ (nm) ($\log \varepsilon\ (M\,l)^{-1}$) in CH_3CN
1	$CHCl_3$	291(4.43), 412(4.00), 655(2.41)
	MeCN	235, 291, 412, 650*
	MeCN + O_x	275, 305*, 325*, 352, 705
	DMF	292(4.37), 412(3.94), 680*(2.22)
	DMF + O_x	276, 310*, 325*, 763, 870*
2	$CHCl_3$	248(sh), 295(4.70), 322**, 416(4.25), 670*(2.35)
	MeCN	232, 295, 415, 668
	MeCN + O_x	279, 305*, 320*, 355, 706
	DMF	293(4.25), 415 (4.12), 675*(2.27)
	DMF + O_x	279, 313, 330*, 359, 747
3	$CHCl_3$	250**, 293(4.54), 324**, 412(4.11), 660*(2.20)
	MeCN	236, 293, 412, 650*
	MeCN + O_x	240, 306*, 325*, 352, 701
	DMF	291(3.47), 413(3.06), 680*(2.25)
	DMF + O_x	274, 306*, 325*, 355, 764, 870*
4	$CHCl_3$	250**, 292(4.82), 337**, 415(4.29), 665*(2.31)
	MeCN	238, 292, 415, 680*
	MeCN + O_x	282, 307*, 325*, 353, 707
	DMF	293(4.68), 415(4.19), 680*(2.29)
	DMF + O_x	276, 306*, 321*, 357, 764, 860*
5	$CHCl_3$	269(4.98), 308(4.83), 430(4.18)
	MeCN	232(4.48), 246(4.46), 293(4.53), 417(4.03), 680*(2.20)
	MeCN + O_x	272, 353, 677
	DMF	292(4.52), 417(4.44), 680*(2.15), 830**(1.69)
	DMF + O_x	276, 300**,330**, 356, 737
6	$CHCl_3$	251(4.59), 293(4.74), 415(4.26), 670*(2.12)
	MeCN	250(4.59), 293(4.74), 415(426), 680*(1.15), 830**(1.66)
	MeCN + O_x	277, 305**, 320**, 352, 707
	DMF	291(4.52), 415(4.00), 670*(2.19), 830**(1.76)
	DMF + O_x	277, 308*, 325*, 746

* Shoulder.
** Very week shoulder.

Table 5
EPR parameters of **1–6** complexes.

Compex	Solid state spectral parameters		Solution spectral parameters					
	g_{II}	$g_\perp$	g_{iso}	g_{II}	$g_\perp$	$^*A_{iso}$	$^*A_{II}$	$^*A_\perp$
1	2.189	2.069	2.124	2.237	2.067	66	166	16.0
2	2.221, $^*A_{II}$ = 128	2.057	2.126	2.238	2.071	68	164	20.0
3	2.198	2.075	2.124	2.232	2.069	69	168	19.0
4	2.223	2.071	2.116	2.232	2.058	69	158	24.4
5	2.228, $^*A_{II}$ = 165	2.054	2.117	2.224	2.036	64	165	13.5
6	2.232, $^*A_{II}$ = 154	2.047	2.116	2.223	2.041	63	166	11.5

* *A* parameters are given in $10^4\ cm^{-1}$.

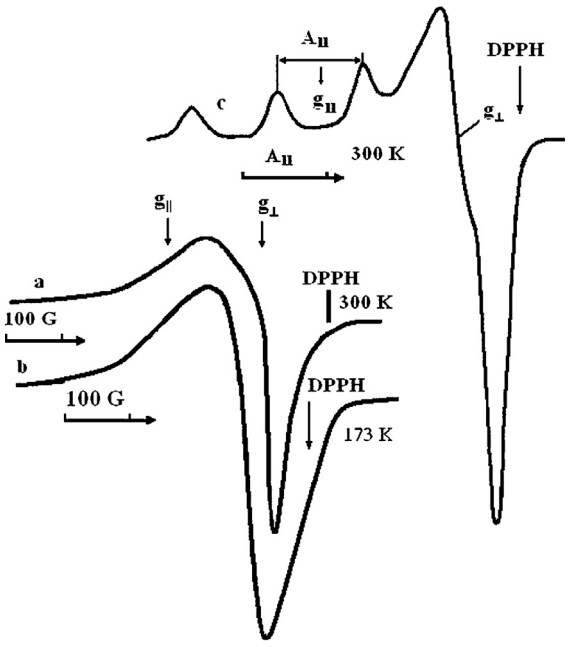

Fig. 3. The powder EPR spectra of **2** (a) at 300 K and (b) 173 K and **6** (c) at 300 K.

spectra for **1**, **3** and **6** complexes are given in Fig. 4. The g_{II} and A_{II} values of these complexes are very similar to each other, indicating that their molecular geometry is governed by the steric effect of salicylaldimine $^{t}Bu_2$ groups. Except **4** ($G = 4.12$), the exchange interaction parameter, $G = (g_{II}-g_e)/(g_{\perp}-g_e)$, values (3.43–3.66) for **1**–**6** complexes being <4 suggest the existence a small exchange coupling between Cu^{II} centers [35]. Another convenient empirical index of tetrahedral distortion, $f(\alpha) = g_{II}/A_{II}$, is regarded as an extent of deviation from idealized planar geometry [36]. The obtained ratio g_{II}/A_{II} for all frozen glass **1**–**6** samples (133–141 cm) falls within the range 130–150 cm and indicate the existence of a slightly tetrahedral distorted geometry around Cu(II) centers in the above complexes [36].

2.3. Electrochemistry

Electrochemical properties of copper complexes were studied on a Pt disc electrode in acetonitrile containing 0.05 M Et_4NBF_4 as the supporting electrolyte. The main electrochemical data of **1**–**6** complexes are given in Table 6. As can be seen from Table 6, all

Table 6
Voltammetric data for the compounds **1**–**6**.

Compound	E_{pa} (V)	E_{pa} (V)	E_{pc} (V)	E_{pc} (V)
1	1.059	0.131	0.098	−0.398
2	1.048	0.366	−0.338	−1.005
3	1.172	0.672	–	−0.762
4	1.071	–	–	–
5	1.134	0.206	0.169	−0.322
6	1.190	–	–	−1.062

Supporting electrolyte = 0.05 M Et_4NBF_4, scan rate = 100 mV/s.

complexes exhibit irreversible oxidation peak within 1.050–1.119 V, which can be assigned to the ligand centered Cu(II)–phenoxide/Cu(II)–phenoxyl couples. Cyclic voltammogram of **1** exhibits an irreversible oxidation peak at 1.059 V (Fig. 5a). The irreversibility suggests the instability of the generated radical species under electrochemical time scale. Interestingly, some more oxidation and reduction waves were generated in the second scan as shown in (Fig. 5b). Complex **1** exhibits an oxidation at 0.131 V and a corresponding reduction peak at 0.098 V. The separation in the peak potentials, ΔEp, is 33 mV indicating a quasi-reversible two electron transfer process which is assigned to the oxidation/reduction of imine moiety of the ligand [37a–c]. Similar electrochemical behavior also was detected for complex **5** (Table 6 and Fig. 6). Interestingly, the anodic peak for **1**–**6** complexes was shifted to more positive values as the number of electron-withdrawing F atoms increased. On the other hand, there is no correlation between the number F atoms and the cathodic peaks values (−0.322/−1.062 V) which are assigned to the reduction of copper(II) to copper(I) (Table 6). The presented electrochemical study indicates that all anodic oxidation processes are ligand centered. These results suggest that the observed chemical oxidation in **1**–**6** complexes are ligands centered. The $Ip/v^{1/2}$ value is almost constant for all scan rates. This establishes the electrode process as diffusion controlled [37d].

2.4. Chemical oxidations of *1*–*6*

The chemical oxidation properties of **1**–**6** were investigated by *in situ* UV/vis spectral measurements in MeCN and DMF. The oxidation of the complexes was carried out with one and two equivalent molar amounts $(NH_4)_2Ce(NO_3)_6$ (CAN). Addition of an equiv. amount of CAN to **1**–**6** in above solvents at r.t. caused a color change from dark brown to green. The spectral changes for **1**–**6** + CAN system were monitored by UV/vis spectroscopy during the progress of their oxidation in CH_3CN and DMF solutions. The

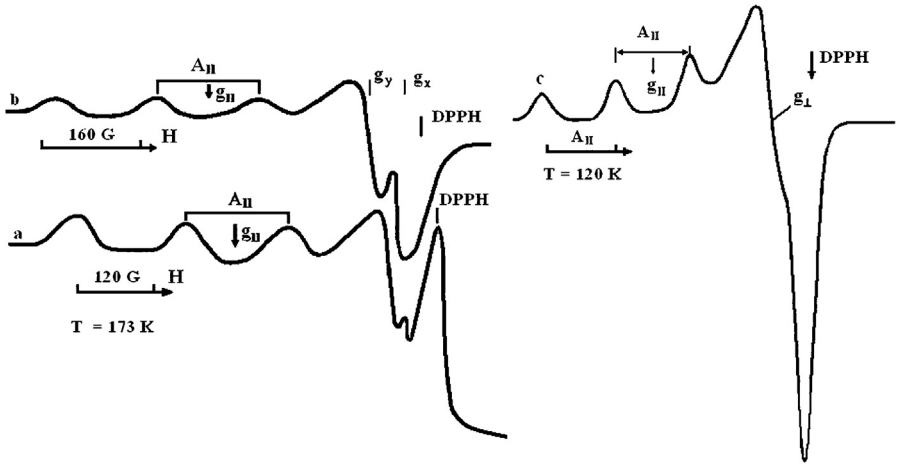

Fig. 4. Frozen glass EPR spectra of **1** (a), 3 (b) (173 K) and **5** (c) (120 K) in $CHCl_3$.

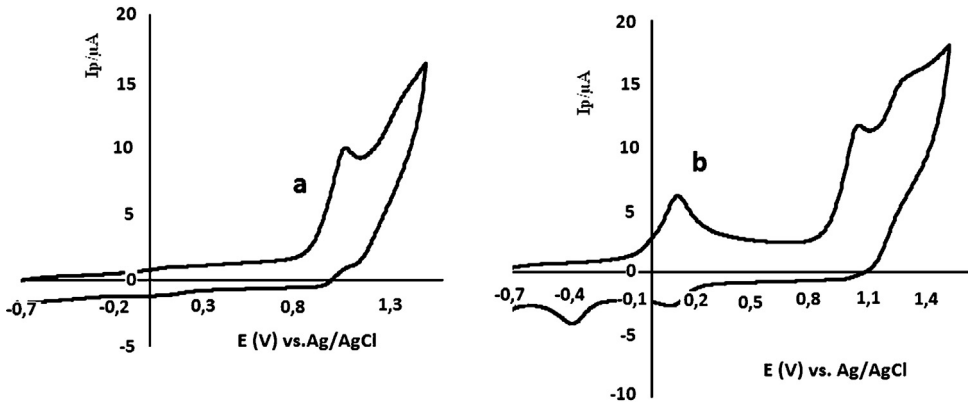

Fig. 5. The cyclic voltammograms of complex **1** in acetonitrile containing 0.05 M Et_4NBF_4 as supporting electrolyte. Scan rate 100 mV/s. First scan (a) and second scan (b).

examination revealed that the redox behavior of complexes **1**–**6** is distinctively different from their non-fluorinated dimethyl [22d] and dimethoxy [23c] substituted analogues and mono substituted (CH_3, CH_3O, F, Cl, Br) bis(*N*-X-Ph-3,5-di-*tert*-butylsalicylaldiminato)-Cu(II) complexes [30c]. On the other hand, the redox feature of the radical intermediates generated from these complexes by using two equiv. of CAN in CH_3CN and DMF are different from each others. Upon one-electron oxidation of **1**–**6** complexes by one or two equiv molar amounts of CAN in MeCN at r.t and aerobic conditions, along with instant disappearance of d–d bands at about 660 nm and LMCT absorptions around 412–415 nm region of the parent complexes, the appearance of a new asymmetric or symmetric broad maximum bands centered within 350–360, 701–707 and 730–770 nm regions, assignable to Cu(II)/Cu(III)–phenoxyl radical species, were observed (Table 4) [2–5,38]. The UV/vis spectral changes accompanied by the oxidations of **1**–**6** are shown in Figs. 7–10. For all **1**–**6** complexes, under above experimental conditions, the decrease in intensities and blue or red shifts in λ_{max} of the first detected bands during the 3–5 successive scanning with a period of 50 s were observed. Upon further scanning, the decrease in the intensity of 701–707 nm (MeCN) and 730–765 nm (DMF) bands for all oxidized species $\mathbf{1}^{+}$–$\mathbf{6}^{+}\bullet$ practically stopped when the oxidation is carried out with one or two equiv of CAN in MeCN and in the case of the oxidation by one equiv of CAN in DMF (Fig. 7). The energy and intensity of these features are consistent with the $\pi \rightarrow \pi^*$ transitions associated with a bisphenoxyl radical species [38]. These bands can be detected even after 24 h under aerobic conditions. However, when the oxidation of complexes **1**–**4** is carried out with two equiv of CAN in DMF, along with above spectral changes, after third or fourth scan the appearance of a new broad maximum band with a slowly growing intensity at *ca.* 730 nm with a shoulder about 870 nm were detected (Figs. 8 and 9 and Table 4). Generally, after the fourth/fifth successive scans, the intensity of new band starts to increase gradually upon further scans of the oxidized reaction mixture and then after about 60–80 min its absorbance again begins to decrease. For example, addition of 2 equiv of CAN to solution **1** (1.14×10^{-2} M) in DMF at r.t., a new asymmetric broad maximum at 765 nm with a shoulder at *ca* 870 nm appears in the spectra of the reaction mixture (Fig. 8A). Upon further successive scans with a period 50 s, the intensity of this band rapidly decreases from 765(2.88), 718(1.35), 700(1.21) to 695(1.21) and then, at forth scan a new band begins to grow at 698(1.39) nm and upon further scanning its intensity is increased to 709(1.99) nm (Fig. 8A). A similar spectral behavior was also observed in the oxidation of **3** (Fig. 8B) and **4** (Fig. 9) complexes by two equiv CAN under the same experimental conditions. In the chemical oxidation of complexes **5** and **6** with 2 equiv CAN in DMF, together with disappearance of their d–d bands, the appearance of new absorptions at 737(2.69) and 746(3.40), respectively, were detected. Upon three successive scans, the intensity of these bands rapidly decreased from 737(2.69) to 750(0.61) nm and from 746(3.40) to 758(0.37) nm, respectively, for $\mathbf{5}^{+}$ (Fig. 10a) and $\mathbf{6}^{+}$ (Fig. 10b). However, after fourth scan with a period of 50 s, the appearance of new weak shoulder band at about 630 nm for both complexes was observed. These bands can be assigned to non radical ligand Cu(II) complexes.

To the best of our knowledge, the observed spectral changes in the chemical oxidation of polyfluorinated Cu(II)–phenoxyl systems by two equivalent of Ce(IV) in DMF is unusual phenomenon. Unfortunately, while there are a wide variety chemical or electrochemical oxidation studies of various transitions metal complexes with di-*tert*-butylphenol function-

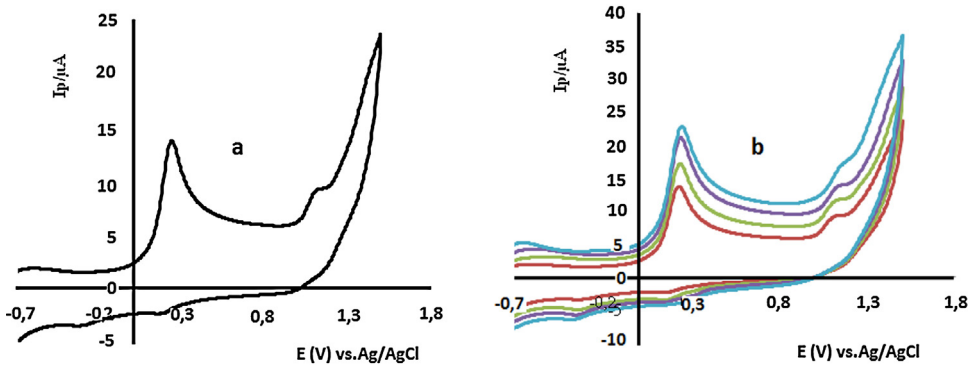

Fig. 6. The cyclic voltammograms of complex **5** in acetonitrile containing 0.05 M Et_4NBF_4 as supporting electrolyte. (a) Scan rate 100 mV/s (first scan) and (b) Scan rates increasing from100 mV/s to 250 mV/s.

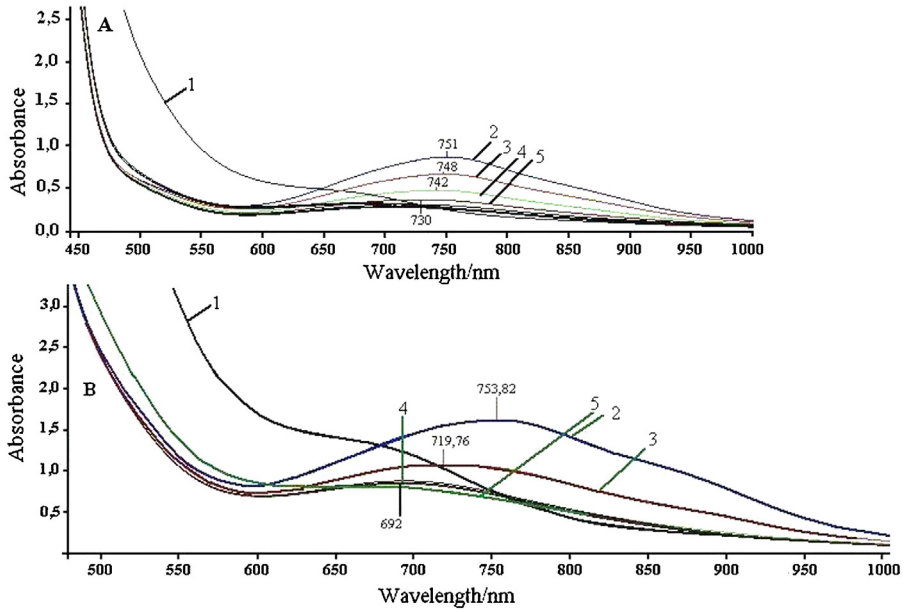

Fig. 7. UV–vis spectral changes in during one-electron oxidation of 1 (7.5×10^{-3} M, (A (1)) and **3** (2.5×10^{-3} M, (B (1) by one equiv of CAN at r.t. in DMF. Spectral changes for $\mathbf{1}^{\bullet\bullet+}$ (A) and $\mathbf{3}^{\bullet\bullet+}$ (B): In both figure number 1 denote spectrum of parent complexes. The numbers 2, 3, 4 are spectra of **1**(**3**) +1 equiv CAN systems scanned with a period 50 s. Spectrum 5 in A and B recorded after 20 h.

alized bi-, tri- and tetradendate non-fluorinated salicylaldimine ligand systems [1–7], we could not find any report in literature similar to spectral changes observed in our study. The fact that secondary spectral changes do not appear in non-fluorinated various di-CH_3 and di-CH_3O substituted *N*-XPh-3,5-DTBS ligands Cu(II) complexes [22d,23c], we suggest that the observed unusual redox behavior may be originates from fluorine atoms.

Thus, the redox-reactivity of the polyfluorinated sterically hindered di-*tert*-butylphenol functionalized **1**–**6** complexes and reactivity of the generated Cu–phenoxyl radicals depends on the number and positions of the fluorine atoms in the aniline ring and solvent nature. The observed spectral changes originate from the conversions of the initially generated Cu-phenoxy radical species to another secondary phenoxy radical species.

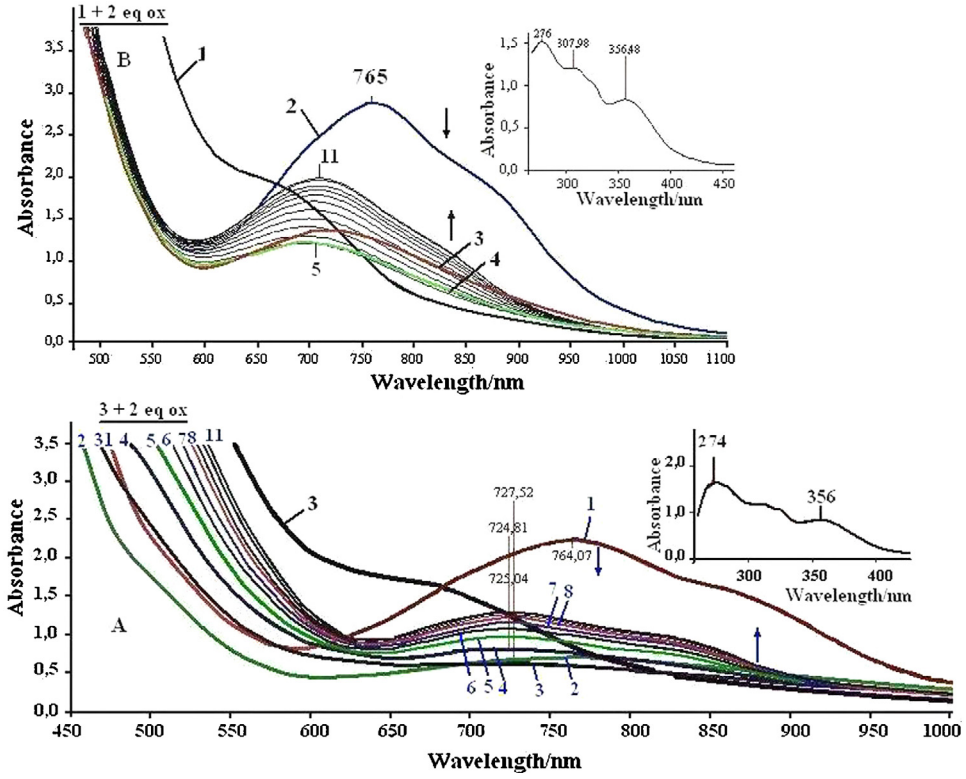

Fig. 8. UV/vis spectral changes during one-electron oxidation of 1 (a) and 3 (b) by two equiv of CAN in DMF solution at r.t. In both, Fig. 1 denotes spectrum of neutral complexes. The intensity of the spectra of **1/3** +2 equiv CAN systems rapidly decreased from 2 to 4 and then upon further scanning with a period 50 s, the appearance of a new spectra which the intensities increase from 5 to 15 (a) and from 5 to 12 (b) were detected. The arrow indicates the direction of the increasing absorbance.

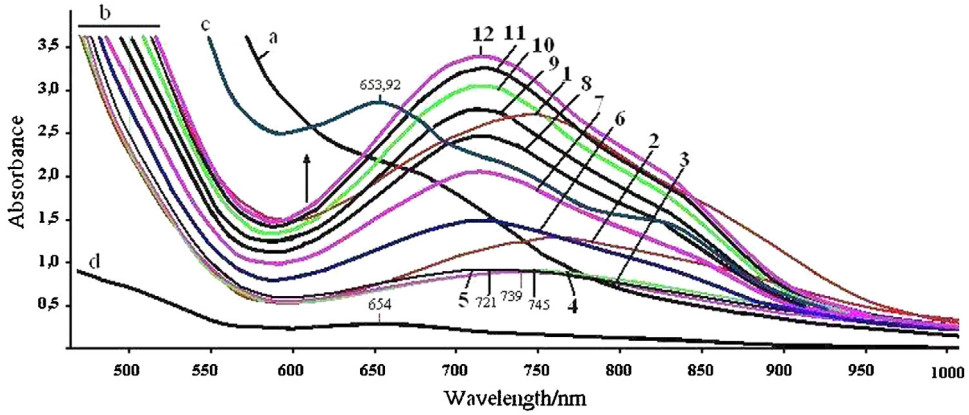

Fig. 9. Visible spectrum of 4 (1.2×10^{-2} M) (a) and spectral changes of 4 + 2 equiv CAN mixture; (b) the 1, 2, 3 and 4 spectra are subsequently scanned in the progress of the chemical oxidation *via* of 50 s; the spectra 5–12 are scanned with a period of 2–10 min; (c) spectrum is scanned after 15 h; (d) spectrum of the dilute solution sample of (c).

2.5. Cytotoxic activity

The cytotoxic effects of ligands **HL^1**–**HL^6**, and their corresponding Cu(II) complexes **1**–**6** were assessed by MTT [(3-(4,5-dimethylthiazol-2-yl)-2,5-diphenyltetrazolium bromide)] assay. K562 cells were treated for 72 h with increasing doses of the ligands and 5-Fluorouracil (5-FU). Upon assessment of viability, IC_{50} (micromolar concentration inhibiting 50% cell growth) values were calculated for compounds **HL^1 (2,4-F$_2$)**, **HL^2 (2,5-F$_2$)**, **HL^3 (2,6-F$_2$)**, **HL^4 (2,3,4-F$_3$)**, **HL^5 (2,3,5,6-F)** and **HL^6 (2,3,4,5,6-F$_5$)**. The IC_{50} values for these ligands were found as 8.78, 91, >100, 2.81, 3.73 and 0.04 μM, respectively. Under the same conditions for reference 5-FU drug, the IC_{50} value was found to be as >100 μM. The compactions of cytotocxic activity data between difluorinated **HL^1**, **HL^2** and **HL^3**, as well as between monofluorinated **HL^7** (*p*-F) and **HL^8** (*o*-F) revealed that their IC_{50} data (Table 7) significantly affected by the positions of F atoms on the aniline ring. Based on the IC_{50} values, pentafluorinated **HL^6** ligand was found to be the most potent cytotoxic one. In addition, according to IC_{50} value of 5-FU and **HL^3** the cytotoxic influence on the K562 cell lines is negligible. Comparison of IC_{50} values of above mentioned ligands strikingly revealed that, in generally, upon increase in the numbers of F atoms in the aniline rings the cytotoxic efficiency of the fluorinated ligands also increases. But in some cases there is a deviation from this trend. It is noteworthy that for 2,4-F$_2$Ph-3-*tert*-butylsalicylaldimine and 2,4-F$_2$Ph-5-*tert*-butylsalicylaldimine compounds, which contains only one *tert*-butyl substituent on the salicylaldimine moiety, the evaluated IC_{50} values were found to be about 16 μM. On the other hand, the analogous non-fluorinated 3,5-di-*tert*-

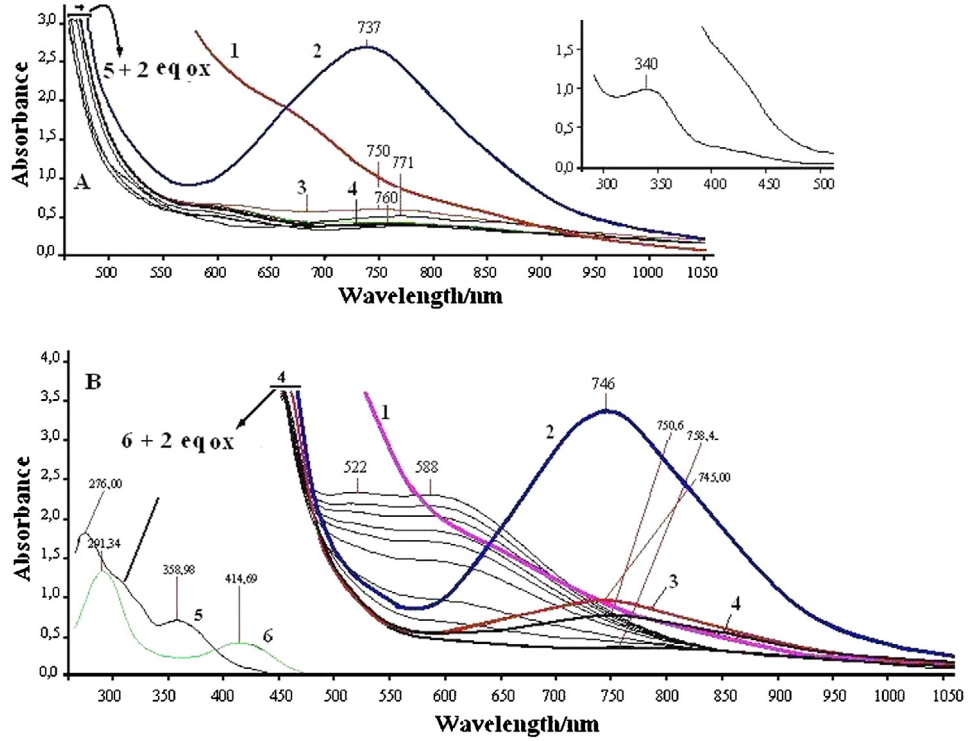

Fig. 10. UV–vis spectral changes in the progress of the one-electron chemical oxidation of **5** (1.26×10^{-2} M, (A (1)) and **6** (9.88×10^{-3} M, (B (1) by two equiv CAN in DMF at r.t. Spectral changes for 5$^{\bullet\bullet+}$ (A) and 6$^{\bullet\bullet+}$ (B) 2, 3 and 4 are 1st, 2nd and 3rd scans of oxidized **5** and **6**, respectively, with a period of 50 s; 5-diluted spectrum of 6$^{\bullet\bullet+}$. 6-diluted solution spectrum of **6**. Inset: Spectrum of the dilute solution samples of 5$^{\bullet+}$.

Table 7
Chemical structure and IC_{50} data for ligands and their Cu(II) complexes.

Chemical structure	HL^x	IC_{50} (μM)	Chemical structure	$Cu(L^x)_2$	IC_{50} (μM)
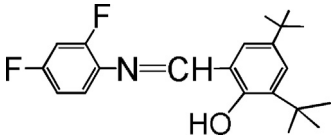	HL^1	8.78	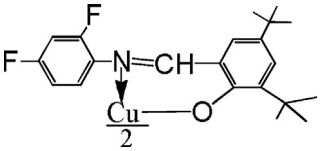	**1**	1.27
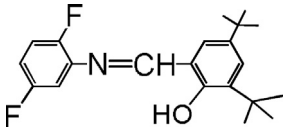	HL^2	91	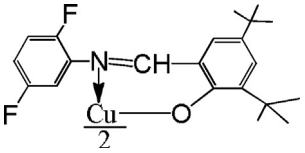	**2**	>100
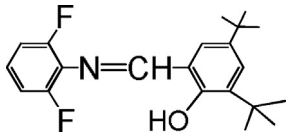	HL^3	>100	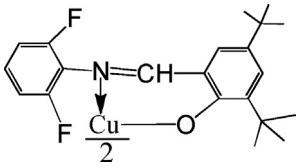	**3**	90
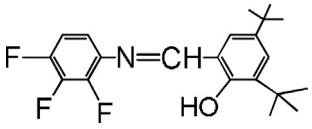	HL^4	2.81	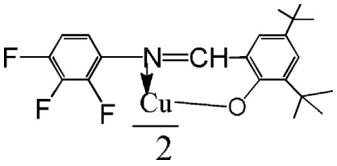	**4**	2.8
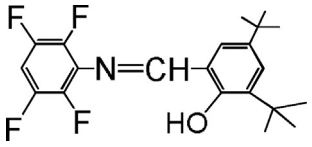	HL^5	3.73	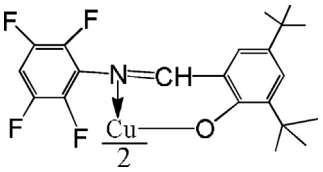	**5**	1.12
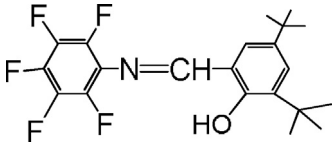	HL^6	0.04	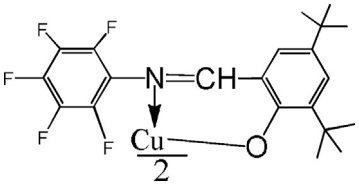	**6**	3.21
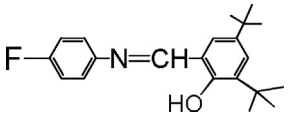	HL^7	348	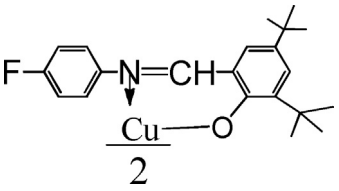	**7**	105
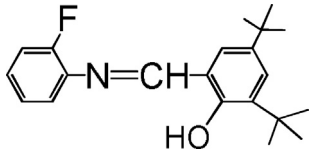	HL^8	30	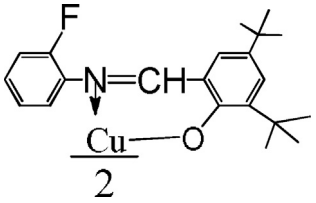	**8**	75
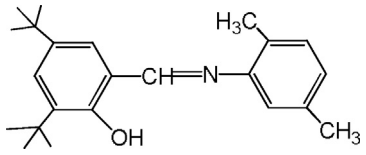	HL^9	745	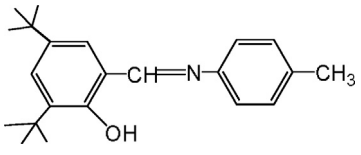	HL^{10}	703

butylsalicylaldimine ligands having various *di*-CH_3 (2,3-, 3,4-, 2,5- and 3,5-di CH_3), 2-CH_3, 4-CH_3 and 4-CH_3O substituents on the aniline rings exhibited negligible (IC_{50} = 568–2078 μM) cytotoxic effects under the same conditions (Table 7). These results demonstrate that the observed cytotoxic effects of HLx Schiff bases originate from the number and positions of fluorine atoms on the aniline rings. In order to investigate the influence of the complexation of the ligands with Cu(II) on their cytotoxic effects under above conditions, for **1–6** complexes, the IC_{50} values were evaluated. The obtained values of IC_{50} for complexes **1–6** were found to be as 1.27, >100, 90, 2.8, 1.12 and 3.21 μM, respectively. These data indicate that the complexation of the **HL^1, HL^4,** and **HL^5** ligands with Cu(II) increase their cytotoxic activities on the K562 cells. Thus, some polyfluorinated redox-active salicyilaldimine ligands and their Cu(II) complexes showed strong cytotoxic effects in comparison with that of 5-FU which showed value $IC_{50} > 100$ against K562 cell lines. While in many cases, it has been found that the biological activity of ligands is increases in their complexation with metal ions [39], in our case a significant increases in the cytotoxic effects for some coordinated ligands have been observed.

3. Conclusions

A new series of polyfluorinated Cu(II) complexes with *N*-polyfluorophenyl-3,5-di-*tert*-butylsalicylaldimine ligands have been prepared and their structure characterized by various spectroscopic, magnetic and X-ray diffraction techniques. UV/vis and EPR spectral studies along with magnetic moment data suggest slightly distorted square-planar geometry for all complexes. X-ray study reveals that the asymmetric unit of **5** contains two crystallographically independent molecules. UV/vis study reveals that the redox properties of the polyfluorinatrd 3,5-*di*-*tert*-butylated Schiff base Cu(II) complexes are greatly affected by the number and the location of the fluorine atom(s) in the phenyl rings. The chemical oxidation of all complexes with one and two equiv of CAN in MeCN or with one equiv of CAN in DMF, leads to the immediate disappearance of d–d bands and the appearance a broad strong band at 730–760 with a shoulder around 850 nm which are assigned to Cu(II)–phenoxyl radical complexes. The intensity of these bands within 2–3 min decreased about %70–80 and upon further scanning their intensity practically remained constant. Unexpectedly, upon chemical oxidation of **1–4** with two equiv of CAN in DMF at r.t. along with above mentioned spectral changes, the appearance of a new bands at around 715–740 nm, assignable to Cu(III)(phenoxyl)(phenolat)NO_3^{-1} radical species, were observed. Upon oxidation of **5** and **6** with two equiv of CAN in DMF, the spectra of the generated radicals after 4 scans gradually converted to another spectra typical for nonradical Cu(II) complexes. The electrochemical oxidation of **1–6** revealed that these complexes possess ligand centered oxidation in the region 1.0–1.2 V. *In vitro* study of cytotoxic activities of the **HL^1–HL^6** and their complexes against K562 cell lines revealed that some of these compounds possess higher (IC_{50} = 0.04–8.78 μM for **HL^x** and 1.12–3.21 μM for **1**, **4**, **5**, **6**) cytotoxic activity. It has been found that as the number of F atoms increases in **HL^x** their IC_{50} values decrease.

4. Experimental

4.1. Materials

All reagents and solvents were obtained commercially and used without further purification. All 2,4-di-*tert*-butylphenol, hexamethylenetetramine, copper(II)acetate monohydrate, $(NH_4)_2Ce(NO_3)_6$ (CAN), acetic acid and all fluorinated anilines (2,4-difluouroaniline, 2,5-difluouroaniline, 2,6-difluouroaniline, 2,3,4-trifluouroaniline, 2,3,5,6-tetrafluouroaniline and 2,3,4,5,6-pentafluouroaniline) reagents were purchased from Sigma-Aldrich. 3,5-^{t}Bu$_2$-salicylaldehyde was prepared according to a published procedure [40].

4.2. Instrumentation

The C, H, N elemental analyses were performed on a LECO CHNS-932 model analyzer. UV/vis spectra were measured on a Perkin-Elmer Lambda 25 spectrometer operating between 200 and 1100 nm. IR spectra were recorded as KBr pellets on a Perkin-Elmer FTIR spectrometer in the 450–4000 cm^{-1} region. The ^{19}F NMR measurements were performed on an Agilent–NMR–VNMRS 400 MHz spectrometer operating at 376 MHz. in $CDCl_3$. ^{19}F NMR chemical shifts were determined relative to $CDCl_3$ as the external standard and low field is positive. EPR spectra were recorded on a Varian model E 109C spectrometer in X-band with 100 kHz modulation frequencies. The *g*-values were determined by comparison with a 2,2-diphenyl-1-picrylhidrazyl (DPPH) of $g = 2.0036$. The room temperature magnetic susceptibility was measured by using a Sherwood Scientific magnetic balance and the diamagnetic corrections were evaluated from Pascal's constants [41]. The phenoxyl radical species of the complexes were generated *in situ* by adding an equimolar amount (1 or 2 equiv amount) of $(NH_4)_2[Ce(NO_3)_6]$ (CAN) ($2{,}5–5.0 \times 10^{-3}$ M) to a solution (DMF or MeCN) of corresponding **1–6** in a UV cell (1-cm path length, with a silicon cap) at r.t. under aerobic conditions. An EcoChemie Autolab-12 potentiostat with the electrochemical software package GPES 4.9 (Utrecht, The Netherlands) was used for voltammetric measurements. A platinum disk (2 mm o.d.) was employed as a working electrode, a platinum coil as a counter electrode, and an Ag/AgCl as reference electrode, respectively. All measurements were performed in MeCN containing 0.05 M Et_4NBF_4 as a supporting electrolyte at room temperature (r.t.) and under nitrogen atmosphere.

4.3. Synthesis of ligands

N-(3,5-di-*tert*-butylsalicylidene)-2,4-difluoroaniline (**HL^1**), *N*-(3,5-di-*tert*-butylsalicyl-idene)-2,5-difluoroaniline (**HL^2**), *N*-(3,5-di-*tert*-butylsalicylidene)-2,6-difluoroaniline (**HL^3**), *N*-(3,5-di-*tert*-butylsalicylidene)-2,3,4-trifluoroaniline (**HL^4**), *N*-(3,5-di-*tert*-butyl-salicylide-ne)-2,3,5,6-tetrafluoroaniline (**HL^5**) and *N*-(3,5-di-*tert*-butylsalicylidene)-2,3,4,5,6-penta-fluoroaniline (**HL^6**) ligands were synthesized according to literature procedures [9,13,23b].

The IR, UV/vis and ^1H NMR spectral data as well as redox-reactivity behaviors of **HL^x** ligands have been presented in recent works [12–17,23]. As the ^{19}F NMR spectra of **HL^x** ligands have not been reported, we present herein fluorine-19 NMR spectral data for above ligands. Analysis of the ^{19}F NMR spectral data of **HL^x** ligands revealed the existence of ^{19}F-^{19}F and ^{19}F–^1H interactions in these compounds. The ^{19}F NMR spectrum of **HL^1**: ^{19}F NMR (376 MHz, $CDCl_3$) δ −112.4 to −112.5 ppm (m, $^3J_{FF}$, $^3J_{FH}$ = 2.8–7.2 Hz, 1F), −120.9 to −121.0 ppm (m, $^3J_{FF}$, $^3J_{FH}$ = 3.2–8.0 Hz, 1F). **HL^2**: ^{19}F NMR (376 MHz, $CDCl_3$) δ −117.6 to −117.7 ppm (m, $^3J_{FH}$, $^3J_{FF}$ = 2.3–8.0 Hz,1F), −131.3 to −131.4 ppm (m, $^3J_{FH}$, $^3J_{FF}$ = 2.8–6.8 Hz, 1F). **HL^3**: ^{19}F NMR (376 MHz, $CDCl_3$) δ −123.3 ppm (*t*, $^3J_{FH}$, $^3J_{FF}$ = 7.2, 7.2 Hz, 2F). **HL^4**: ^{19}F NMR (376 MHz, $CDCl_3$) δ −136.6 to −136.7 ppm (m, $^3J_{FH}$, $^3J_{FF}$ = 2.8–6.0 Hz, 1F), −145.4 to 145.6 ppm (dt, 1F) $^3J_{FH}$, $^3J_{FF}$ = 2.8–8.0 Hz 30.4 Hz), −158.5 to −158.6 ppm (td, $^3J_{FH}$, $^3J_{FF}$ = 4.4, 20.4 Hz, 1F). **HL^5**: ^{19}F NMR (376 MHz, $CDCl_3$) δ −139.3 to −139.6 ppm (q, $^3J_{FH}$, $^3J_{FF}$ = 6.8–12.8 Hz, 2F), −152.5 to −152.6 ppm (m, $^3J_{FH}$, $^3J_{FF}$ = 2.8–8.8 Hz, 2F). **HL^6**: ^{19}F NMR, (376 MHz, $CDCl_3$) δ −152.2 to −52.3 ppm (dd, $^3J_{FF}$ = 7.2, 17.0 Hz, 2F), −158.9 to −159.0 ppm (t, $^3J_{FF}$ = 23.2, 21.6 Hz, 1F), −162.55 to −162.7 ppm (td, $^3J_{FF}$ = 7.2, 5.6, 5.6 Hz, 2F).

4.4. Synthesis of **1**–**6** copper(II) complexes

Complexes **1**–**6** were prepared using following general procedure. To a stirring solution of the ligand (1 mmol) in MeOH (50–60 ml) at *ca.* 60 °C a solution of copper acetate monohydrate (0.5 mmol, 0.1 g) in MeOH (10 ml) was added. The resulting dark green solution was refluxed with stirring for 1.0–1.5 h and then was concentrated to ca. 30 ml. After cooling to r.t. the formed microcrystalline solid was filtered off, washed with methanol and dried in air. The copper(II) complexes were recrystallized from chloroform/methanol mixture (yields 68–85%). Ligand **HL**^{4} and its complex **4** are recently reported by us [23b]. However, because their detailed redox reactivity and anticancer behavior have not been reported, for comparative properties, these compounds have been included in present study.

1. Yield 68%. *M.p.* > 280 °C. *Anal.* Calc. for $C_{42}H_{48}N_2O_2F_4Cu$: C, 67.05; H, 6.43; N, 3.72%. Found: C, 66.81; H, 6.53; N, 3.48%. IR (ν cm^{-1}, KBr): ν(C–H) of ^{t}Bu 2867–2963; ν(C=N) 1618; new strong band at 1525 assigned to ν(C–O) + ν(C=C–O); ν(C–O) 1324; ν(Cu–N) 536, 568; ν(Cu–O) 449, 492. μ_{eff} = 1.69μ_B at r.t.
2. Yield 77%. *M.p.* 231 °C. *Anal.* Calc. for $C_{42}H_{48}N_2O_2F_4Cu$: C, 67.05; H, 6.43; N, 3.72%. Found: C, 66.95; H, 6.32; N, 3.68%. IR (ν cm^{-1}, KBr): ν(C–H) of ^{t}Bu 2867–2963; ν(C=N) 1618; new band 1533 assigned to ν(C–O) + ν(C=C–O); ν(Cu–N) 446, 498; ν(Cu–O) 536, 568. μ_{eff} = 1.72μ_B at r.t.
3. Yield 77%. *M.p.* > 280 °C. *Anal.* Calc. for $C_{42}H_{48}N_2O_2F_4Cu$: C, 67.05; H, 6.43; N, 3.72%. Found: C, 66.85; H, 6.59; N, 3.62%. IR (ν cm^{-1}, KBr): ν(C–H) of ^{t}Bu 2867–2964; ν(C=N) 1613; new band at 1525 assigned to ν(C–O) + ν(C=C–O); ν(Cu–N) 506, 497; ν(Cu–O) 534, 519. μ_{eff} = 2.08μ_B at r.t.
4. Yield 67%. *M.p.* 276 °C. *Anal.* Calc. for $C_{42}H_{44}N_2O_2F_8Cu$: C, 61.19; H, 5.38; N, 3.40%. Found: C, 60.97; H, 4.98; N, 3.32%. IR (ν cm^{-1}, KBr): ν(C–H) of ^{t}Bu 2870–2958; ν(C=N) 1615; new band at 1531 assigned to ν(C–O) + ν(C=C–O); ν(Cu–N) 540, 487; ν(Cu–O) 595, 576μ_{eff} = 1.86μ_B at r.t.
5. Yield 67%. *M.p.* 252 °C. *Anal.* Calc. for $C_{42}H_{42}N_2O_2F_{10}Cu$: C, 58.64; H, 4.92; N, 3.25. Found: C, 58.90 H, 4.75; N, 3.06%. IR (ν cm^{-1}, KBr): ν(C–H) of ^{t}Bu 2870–2959; ν(C=N) 1614; new band at 1531assigned to ν(C–O) + ν(C = C–O); ν(Cu–N) 540, 487; ν(Cu–O) 595, 576. μ_{eff} = 1.80μ_B at r.t.

4.5. X-ray structural determination of **5**

Single crystal X-ray diffraction was carried out at 293(2) K using a Bruker APEX-II CCD diffractometer. The intensity data were collected using graphite monochromated Mo *K*α (λ = 0.71073 Å) radiation. The lattice parameters were determined by the least-squares methods on the basis of all reflections with $F^2 > 2\sigma(F^2)$. Integration of the intensities, correction for Lorentz and polarization effects and cell refinement was performed using Bruker AXS APEX II software suit [42]. The structures were solved by direct methods using SHELXS-97 [43] and refined by a full-matrix least-squares procedure using the program SHELXL-97 [43]. H atoms were positioned geometrically and refined using a riding model. The final difference Fourier maps showed no peaks of chemical significance. The molecular structure plots were prepared using ORTEP III [44]. The crystal and structural data for complex **5** are given in Table 1.

4.6. K562 cell line and proliferation assay

MTT [(3-(4,5-dimethylthiazol-2-yl)-2,5-diphenyltetrazolium bromide)] assay were used for IC_{50} determination. K562 (human chronic myelogenous leukemia) cells in exponential growth stage were harvested from culture and centrifuging at 1800 rpm for 10 min, and resuspended in fresh medium at a cell density 3×10^4 cells/ml. The cell suspension was seeded per well in 96-well microplate in triplicate order. Each well was cultured at 37 °C under 5% CO_2 in RPMI1640 medium supplemented with %10 fetal calf serum (FCS) 72 h with 5-Fluorouracil (5-FU) or ligands (**HL**^{1}–**HL**^{6}) and their respective Cu(II) complexes (**1**–**6**) that the concentrations ranged from 31.25 μM to 1000 μM as serial 1:2 dilutions. Then MTT solution (diluted phosphate buffered saline, 5 mg/ml, 10 μl) was added to each well and incubated for 4 h. The formazan crystals were dissolved by adding DMSO (100 μl) to each well after centrifuged for 10 min under 1800 rpm, and the absorbance valued was measured at 570 nm.

Acknowledgments

Harra University Research Fund (HUBAK, Project Number 712) and the Scientific and Technological Research Council of Turkey (TUBITAK, Project Number: ARDEB-113Z134) are kindly acknowledged for financial support.

Appendix A. Supplementary data

Supplementary material related to this article can be found, in the online version, at http://dx.doi.org/10.1016/j.jfluchem.2014.03.011.

References

[1] C.G. Pierpont, C.W. Lange, in: K.D. Karlin (Ed.), Prog. Inorg. Chem. 41 (1994) 331–442.
[2] P. Chaudhuri, K. Wieghardt, Prog. Inorg. Chem. 50 (2001) 151–216.
[3] B.A. Jazdzewski, W.B. Tolman, Coord. Chem. Rev. 200 (2000) 633–685.
[4] J.W. Whittaker, Chem. Rev. 103 (2003) 2347–2364 (and references therein).
[5] J. Stubbe, W.A. van der Donk, Chem. Rev. 98 (1998) 705–762.
[6] V.C. Gibson, S.K. Spitzmesser, Chem. Rev. 103 (2003) 283–315.
[7] L. Canali, D.C. Sherrington, Chem. Soc. Rev. 28 (1999) 85–93.
[8] H. Makio, N. Kashiwa, T. Fujita, Adv. Synth. Catal. 344 (2002) 477–493.
[9] R. Furuyama, J. Saito, S. Ishii, H. Makio, M. Mitani, H. Tanaka, T. Fujita, J. Organomet. Chem. 690 (2005) 4398–4413.
[10] H. Makio, H. Terao, I. Washita, T. Fujita, Chem. Rev. 111 (2011) 2363–2449.
[11] A.F. Mason, G.W. Coates, J. Am. Chem. Soc. 126 (2004) 16326–16327.
[12] A. Sakuma, M.S. Weiser, T. Fujita, Polym. J. 39 (2007) 193–207.
[13] M. Mitani, R. Furuyama, J. Mohri, J. Saito, S. Ishii, H. Terao, T. Nakano, H. Tanaka, T. Fujita, J. Am. Chem. Soc. 125 (2003) 4293–4305.
[14] (a) T. Matsugi, T. Fujita, Chem. Soc. Rev. 37 (2008) 1264–1277;
(b) A.F. Mason, G.W. Coates, J. Am. Chem. Soc. 126 (2004) 16326–16327;
(c) D.P. Song, Y.G. Li, R. Lu, N.H. Hu, Y.S. Li, Appl. Organ. Chem. 22 (2008) 330–340.
[15] K. Kawai, T. Fujita, Top. Organomet. Chem. 26 (2009) 3–46.
[16] T. Matsugi, T. Fujita, Chem. Soc. Rev. 37 (2008) 1264–1277.
[17] M. Mitani, J. Mohri, Y. Yoshida, J. Saito, S. Ishii, K. Tsuru, S. Matsui, R. Furuyama, T. Nakano, T. Fujita, J. Am. Chem. Soc. 124 (2002) 3327–3336.
[18] (a) N. Iwasa, S. Katao, J. Liu, M. Fujiki, Y. Furukawa, K. Nomura, Organometallics 28 (2009) 2179–2187;
(b) S. Chen, C. Guo, L. Liu, H. Xu, J. Dong, Y. Hu, Polymer 46 (2005) 11093–11098;
(c) S. Reinartz, A.F. Mason, E.B. Lobkovsky, G.W. Coates, Organometallics 22 (2003) 2542–2544.
[19] T. Hiyama, in: H. Yamamoto (Ed.), Organofluorine Compounds. Chemistry and Application, Springer, Berlin, 2000, pp. 137–182.
[20] (a) P. Jeschke, Chem. Biol. Chem. 5 (2004) 570–589;
(b) R.K. Filler, Y. Kobayashi (Eds.), Biomedical Aspects of Fluorine Chemistry, Kodama Ltd, Elsevier, Tokyo, Amsterdam, 1982;
(c) R. Li, R.L. Smith, H.I. Kenttämaa, J. Am. Chem. Soc. 118 (1996) 5056–5061.
[21] (a) D.B. Harper, D. O'Hagan, Nat. Prod. Rep. 11 (1994) 123–133;
(b) T. Tsuzuki, N. Shirasawa, T. Suzuki, S. Tokita, Adv. Mater. 15 (2003) 1455–1458;
(c) G. Theodoridis, Advances in Fluorine Science, 2, Elsevier, Amsterdam, 2006, pp. 121–175;
(d) D. Chopr, T.N.G. Row, Cryst. Eng. Commun. 13 (2011) 2175–2186.
[22] (a) A.A. Medzhdov, V.T. Kasumov, H.S. Mamedov, Koord. Khim. 7 (1981) 66–71;
(b) V.T. Kasumov, A.A. Medzhidov, Russ. J. Coord. Chem. 21 (1995) 783–787;
(c) V.T. Kasumov, F. Köksal, Y. Zeren, Spectrochim. Acta, A: Mol. Biomol. Spectrosc. 63 (2006) 330–336.
[23] (a) O. Celik, V.T. Kasumov, E. Sahin, Acta Crystallogr. E65 (2009) o2786;
(b) V.T. Kasumov, I. Ucar, A. Bulut, J. Fluorine Chem. 131 (2010) 59–65;
(c) V.T. Kasumov, E. Sahin, Spectrochim. Acta, A: Mol. Biomol. Spectrosc. 107 (2013) 31–38.

[24] (a) M.D. Mulican, M.W. Wilson, D.T. Conner, C.R. Kostlan, D.J. Schrier, R.D. Dyer, J. Med. Chem. 36 (1993) 1090–1099;
(b) I. Leventis, I. Andreadou, A. Papalois, I. Sfiniadakis, V. Gorgoulis, D. Korkolis, D. Hadjipavlou-Litina, P. Kourounakis, C. Fotiadis, In Vivo 18 (2004) 161–169;
(c) V. Weber, C. Rubat, E. Duroux, C. Lartigue, M. Madesclaire, P. Coudert, Bioorg. Med. Chem. 13 (2005) 4552–4564.
[25] (a) T. Maki, Y. Araki, Y. Ishida, O. Onomura, Y. Matsumura, J. Am. Chem. Soc. 123 (2001) 3371–3372 (and references therein);
(b) M. Roberti, D. Pizzirani, M. Roberti, D. Pizzirani, D. Simoni, R. Baruchello, C. Bonora, F. Buscemi, S. Grimaudo, M. Tolomeo, J. Med. Chem. 46 (2003) 3546–3554;
(c) K. Azuma, M. Nakayama, M. Koshioka, Ki Ippoushi, Y. Yamaguchi, K. Kohata, Y. Yamauchi, H. Ito, H. Higashio, J. Agric. Food Chem. 47 (1999) 3963–3966;
(d) V. Dinoiu, Rev. Roum. Chim. 51 (2006) 1141–1152.
[26] J.M. Fernandez, E.A. Aruaz, R.C. Rosado, R.A. Toscano, Transition Met. Chem. 24 (1999) 18–24.
[27] (a) A.D. Garnovski, A.P. Sadimenko, M.C. Sadimenko, D.A. Garnovski, Coord. Chem. Rev. 173 (1998) 31–77;
(b) S. Yamada, Coord. Chem. Rev. 190–192 (1999) 537–555.
[28] A.F. Marinovich, R.S. O'Mahony, J.M. Waters, T.N.M. Waters, Croat. Chem. Acta 72 (1999) 685–703.
[29] J.U. Ahmed, M.T. Raisanen, M. Nieger, P.J. Figiel, M. Leskela, T. Repo, Polyhedron 38 (2012) 205–212.
[30] (a) V.T. Kasumov, F. Köksal, A. Sezer, Polyhedron 24 (2005) 1203–1211;
(b) V.T. Kasumov, F. Köksal, A. Kutluay, Spectrochim. Acta, A 76 (2010) 99–106;
(c) V.T. Kasumov, F. Köksal, R. Köseoğlu, J. Coord. Chem. 57 (2004) 591–603.
[31] (a) G.C. Percy, D.A. Thorpton, J. Inorg. Nucl. Chem. 35 (1973) 2319–2327;
(b) S.J. Gruber, C.M. Harris, E. Sinn, J. Inorg. Nucl. Chem. 30 (1968) 1805–1830.
[32] (a) M. Fores, M. Duran, M. Sola, Chem. Phys. 234 (1998) 1;
(b) G.L. Estiu, A.H. Jubert, J. Costamagna, J. Mol. Struct. 367 (1996) 97–110;
(c) J.M. Downes, J. Whelan, B. Bosnich, Inorg. Chem. 20 (1981) 1081–1086.
[33] (a) A.C. Braithwaite, T.N. Waters, J. Inorg. Nucl. Chem. 35 (1973) 3223–3229;
(b) S. Di Bella, I. Fragala, I. Ledoux, T.J. Marks, J. Am. Chem. Soc. 117 (1995) 9481–9485;
(c) A. Bencini, I. Bertini, D. Gatteschi, A. Scozzafava, Inorg. Chem. 17 (1978) 3194–3197.
[34] (a) A. Earnshaw, Introduction to Magneto Chemistry, Academic Press, London and New York, NY, 1968;
(b) W.E. Hatfield, J.A. Barnes, D.Y. Jeter, R. Whyman, E.R. Jones Jr., J. Am. Chem. Soc. 92 (1970) 4982–4984;
(c) W.E. Marsh, K.C. Patel, W.E. Hatfield, D.J. Hodgson, Inorg. Chem. 22 (1983) 515–544;
(d) E. Colacio, M. Ghazi, R. Kiveka1s, J.M. Moreno, Inorg. Chem. 39 (2000) 2882–2890.
[35] (a) B.J. Hathaway, A.A.G. Tomlinson, Coord. Chem. Rev. 5 (1970) 1–43;
(b) B.J. Hathaway, D.E. Billing, Coord. Chem. Rev. 6 (1970) 143–207;
(c) I.M. Procter, B.J. Hathaway, P. Nicholls, J. Chem. Soc. A: Inorg. Phys. Theor. (1968) 1678–1684.
[36] U. Sakaguchi, A.W. Addison, J. Chem. Soc., Dalton Trans. (1979) 600–608.
[37] (a) A.A. Isse, A. Maye, E. Vianello, J. Electroanal. Chem. 431 (1997) 249–255;
(b) J.E. Kuder, H.W. Gibson, D. Wychick, J. Org. Chem. 40 (1975) 875–879;
(c) B. Ward, C.K. Chang, R. Young, J. Am. Chem. Soc. 106 (1984) 3943–3950;
(d) A.J. Bard, L.R. Faulkner (Eds.), Electrochemical Methods: Fundamentals and Applications, second ed., Wiley, New York, NY, 2001.
[38] (a) J.A. Halfen, B.A. Jazdzewski, S. Mahapatra, L.M. Berreau, E.C. Wilkinson, L. Que, W.B.J. Tolman, J. Am. Chem. Soc. 119 (1997) 8217–8227;
(b) Sokolowski, H. Leutbecher, T. Weyhermüller, R. Schnepf, E. Both, E. Bill, P. Hildebrandt, K. Wieghardt, J. Biol. Inorg. Chem. (1997) 444–453.
[39] (a) H.G. Petering, H.H. Buskirk, G.E. Underwood, Cancer Res. 24 (1964) 367–372;
(b) L.A. Saryan, E. Ankel, C. Krishnamurti, D.H. Petering, H. Elford, J. Med. Chem. 22 (1979) 1218–1221;
(c) M. Christlieb, H.S.R. Struthers, P.D. Bonnitcha, A.R. Cowley, J.R. Dilworth, J. Chem. Soc., Dalton Trans. (2007) 5043–5054;
(d) W. Hernández, J. Paz, F. Carrasco, A. Vaisberg, J. Manzur, E. Spodine, L. Hennig, J. Sieler, L. Beyer, Naturforschung 65b (2010) 1271–1278.
[40] J.F. Larrow, E.N. Jacobsen, Y. Gao, Y. Hong, X. Nie, C.M. Zepp, J. Org. Chem. 59 (1994) 1939–1942.
[41] R.S. Drago, Physical Methods in Chemistry, W.B. Saunders Company, Philadelphia, London, Toronto, 1977.
[42] Bruker, SADABS, Bruker AXS Inc., Madison, WI, 2007.
[43] G.M. Sheldrick, Acta Crystallogr. A64 (2008) 112–122.
[44] L.J. Farrugia, J. Appl. Crystallogr. 30 (1997), 565–565.